CO_2 sorption from a mixture of N_2/CO_2 using an activated carbon and silica gel: equilibrium, breakthrough and mass transfer zone

Mohammed K. Al Mesfer[1], Mohd Danish[1], Basem Abdullah Al Alwan[1], Nasser Sayed Awwad [2]

[1]Chemical Engineering Department, College of Engineering, King Khalid University, 61411 Abha, K.S.A

[2] Chemistry Department, College of Science, King Khalid University, 61411Abha, K.S.A

*Corresponding author:

E-mail: danishmohd111@yahoo.com, Tel: +966580540101

GRAPHICAL ABSTRACT

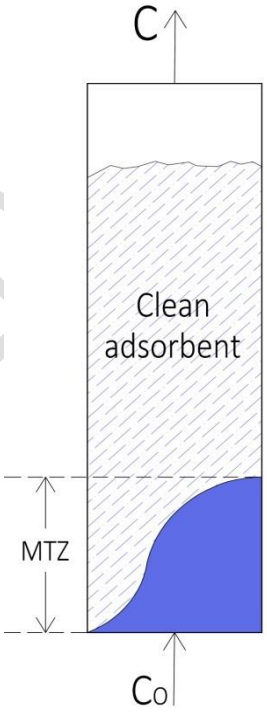

ABSTRACT

The temperature, feed rate, length of mass transfer zone, utilization factor and partial pressure are the parameters considered for fixed bed sorption of CO_2 from N_2/CO_2 mixture. The breakthrough time relies strongly on the temperature and feed rate. The prolonged breakthrough and saturation times have

been realized for AC. The response curves of AC are vastly steep signifying the maximal utilization of bed capacity at the breakpoint. In general, the length of MTZ increases with raised temperature and feed flow rate. The capacity utilization factor reduces with raised temperature and feed flow rate. A utilization factor of 0.919 was determined for AC. The maximal capacity for CO_2 reduces significantly with an increased temperature. The maximal capacities of 32.99 gm CO_2/Kg was determined at a temperature of 298 K for AC. The capacity improves considerably with CO_2 partial pressure and AC exhibited higher adsorption capacity compared to SG. The capacity improves considerably with increased feed rates and maximal capacity of 39.14 g CO_2/Kg adsorbent was determined for AC at the feed rate of 8.33 $x10^{-3}$ m^3/sec. Owing to higher sorption capacity and utilization factor, the AC may be used for economical separation of CO_2 from N_2/CO_2 mixture.

Keywords: sorption, utilization factor, breakthrough, mass transfer zone, capacity

1. Introduction

The combustion of fossil fuels accounts for almost 81% of energy used for commercial purposes, and it releases 3.0 x 10^{13} Kg of carbon dioxide per year (Hester and Harrision, 2010). The prime environmental issue concerns with the alarming rate at which the carbon dioxide concentration is rising in the atmosphere (Li *et al*., 2013; Rashidi *et al*., 2016). The power generation sector between the years 2000 to 2030 will have contributed to almost the total increase in global CO_2 emissions (IEA, 2003). As much as 45% of the total global CO_2 emission is attributed to thermoelectric and industrial electricity generating plants (Lee and Park, 2015).

The mean global temperature rise by just 2^{o}C will result in far-reaching consequences. Therefore, it is recommended that the greenhouse gases be reduced to 50% by the year 2050 (IPCC, 2001). The CO_2 emissions can be reduced by one of the three methods relying on the plant configuration (Alabadi *et al.*, 2015). The treatment of synthesis gas primarily made up of CO and H_2 gases is performed in the pre-combustion process (Figueroa *et al.*, 2008). Approximately 1.5 times more energy is required in the post-combustion process compared to the pre-combustion method of CO_2 capture (Gibbins and

Chalmers, 2008). Primarily, CO_2 and H_2O are the emissions of the oxy-fuel combustion (Blomen *et al.,* 2009).

There are primarily four technologies available for CO_2 reduction from the emissions of power plants based on fossil fuel. Chemical and physical absorption is realized by a reaction between CO_2 and solvent, primarily the amines solutions (Choi *et al.,* 2009). Amine solutions were utilized for CO_2 absorption from CO_2/air mixture and a capacity of 98.2 x 10^{-2} mol/mol was reported for DEA (Gomes *et al.,* 2015). The streams having CO_2 concentration of more than 50% were normally treated using cryogenic separations (Gupta *et at.,* 2003). In the case of CO_2 concentration being more than 20%, the membrane systems are extremely adaptable (Brunetti *et al.,* 2010). The post-combustion CO_2 diminution is mainly a pragmatic process due to the fact that various suggested technologies can be back fitted to existing plants based on fossil fuel (Yang *et al.,* 2008; MacDowell *et al.,* 2010; Cohen *et al.,* 2011). Adsorption is considered as a well-established technology to capture CO_2 in the post combustion process (Garcia *et al.,* 2011; Valverde *et al.,* 2011) The adsorbent preferentially separates CO_2 and afterwards regenerates to release the CO_2 irrespective of the process configuration (Li *et al.,* 2011; Alonso *et al.,* 2010).

Fine activated carbons have been employed under sound assisted fluidization for CO_2 capture, and the experiments reported enhanced adsorption (Raganati *et al.,* 2015). Fluidized bed column was utilized to analyze the separation of CO_2 from flue gas feed experimentally (Abanadas *et al.,* 2004; Valverde *et al.,* 2012). In-depth study of breakthrough behavior was conducted utilizing activated carbon beads (Shen *et al.,* 2011). The activated carbons, zeolites and molecular sieve were employed to explore the kinetics and equilibrium (Sarkar *et al.,* 2017). The effect of superficial velocity on breakthrough response utilizing MOF, activated carbons and crystalline pellets was investigated (Al-Janabi *et al.,* 2018). The beads of activated carbons were utilized to examine the adsorption equilibrium with feed mixture of CO_2 and N_2 (Shen *et al.,* 2010). A MOF (UTSA-16) was utilized for CO_2 separation, and the maximal adsorption capacity of $1.60x10^2$ cm^3/cm^3 was reported (Xing *et al.,* 2012). The adsorption

response of polyaspartamide was predicted using models based on kinetics, and it was concluded that an adsorption is credited to external mass transfer (Yoro *et al.,* 2017). An adsorption of CO_2 employing various adsorbents has been examined and the maximal capacity was reported for activated carbons (Lu *et al.,* 2008). The parametric study and breakthrough behavior by utilizing two grades of activated carbons employing fixed bed column have been conducted (Al Mesfer *et al.,* 2018; Al Mesfer and Danish, 2018).

Investigators have used Macadamia shell biomass to prepare activated carbons by microwave irradiation technique (Dejang *et al.,* 2015). Additionally, walnut shell has also been used to synthesize activated carbon and employed for manufacturing the cartridge (Jahangiri *et al.,* 2012). An activated carbon fiber was prepared, and a capacity of 1.3 $x10^{-3}$ mol/gm adsorbent was achieved (Calvo-Munoz *et al.,* 2016). The capacity of 9.09 x 10^{-3} mol/gm was reported for synthesized activated adsorbent prepared by treating coal with KOH (Toprak and Kopak, 2017). Activated carbons/N-enriched activated carbons were utilized for CO_2 separation and replicated the breakthrough curve satisfactorily (Dantas *et al.,* 2010). A synthesized adsorbent of 13 X and activated carbon was used for CO_2 separation, and determined a capacity of 2.63 mmol/gm (Regufe *et al.,* 2018).

The optimal incorporation of carbon nanotubes into the zeolites 13 X was carried out, and the increased adsorption capacity was reported (Qasem *et al.,* 2017). Microporous biochar adsorbent was employed for the capture of adsorbate in a fixed bed for experimental and simulation study (Plaza et al., 2016). The amine adsorbents were synthesized using fly ash, and the increased capacity of PEI/FA type-adsorbents was reported (Zhang *et al.,* 2014). The prolonged breakpoint time equal to 350 sec with a capacity of 0.63 mmol CO_2 /gm AC for AC-PKS/CeO_2 has been reported (Hidayu and Muda et al., 2017). Researchers have used walnut and almond shell to synthesize the activated carbons and the internal structure was analyzed using SEM and FTIR (Patil *et al.,* 2013). Walnut shell-based biomass has been converted into activated carbons, and KOH was reported as the prime favorable activation agent (Xia *et al.,* 2016). The chemical activation method (Mataji and Khoshandam, 2014) was applied

to prepare activated carbons from walnut shell biomass, and adsorption capability of the removal of benzene was explored using $ZnCl_2/H_3PO_4$. The aim of the current work is to study the adsorption response of activated carbon (AC) and silica gel (SG). The sorption response will be analyzed using temperature, feed rate, length of mass transfer zone, utilization factor and partial pressure as the parameters.

2. Experimental

2.1. Chemicals

The activated carbon (AC) with size range 0.4-0.8 cm was procured from Fluka analytical and dried at 110 ^oC in the drying oven before the experimental works. The silica gel (SG) with average size range 0.2 to 0.4 cm was procured from GCC laboratory reagent (UK) and dried at a temperature of 120 ^oC before the experimental work. The selected adsorbents were used for experiments as such without any further treatment.

2.2. Setup Diagram

The setup sketch of the adsorption column (effectual length- 24 cm) used for experiments has been shown in Figure 1. The column is made up of stainless steel and jacketed to allow the hot water flow to attain the desired temperature. Flow controllers F_1, F_2 and F_3 measure and control the flow of N_2, CO_2 and CO_2 flow to IR sensor respectively. There are 6 thermocouples positioned along the axial direction of the column.

2.3. Procedure

The gaseous mixture of known composition consisting of CO_2 and N_2 enters at the bottom of the column. The flow of CO_2 and N_2 were controlled by the flow controllers F_1 and F_2. The heating jacket was used to control the desired bed temperature and PID controller incorporated in the control console accomplished the task of fixing the desired temperature. The column exit concentration was measured using IR sensor.

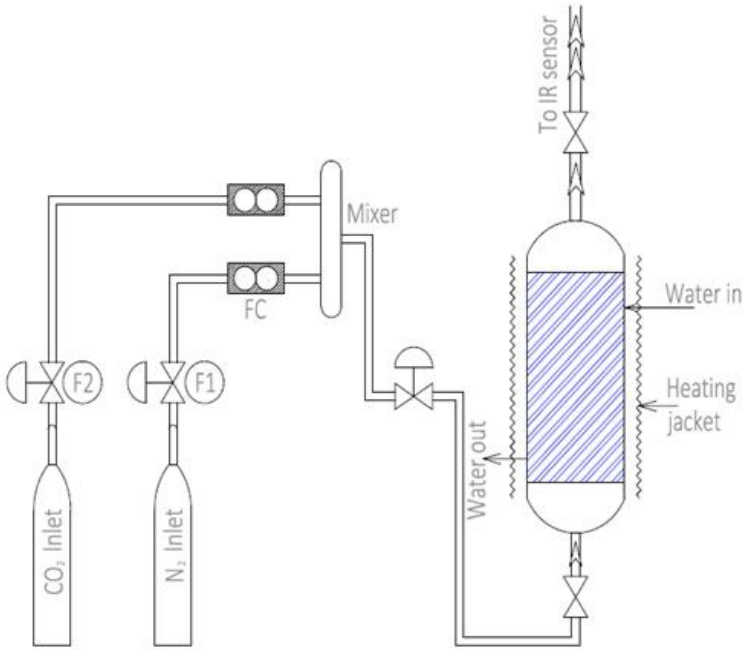

Figure 1. Setup diagram of sorption unit

3. Results and Discussion

3.1. Adsorbent surface characterization

Surface area characterization of both the AC and SG was carried out using surface analyzer (Quantachrome NoavaWin-NOVA Instruments). The results obtained are summarized and depicted in Table 1. The single point surface areas of 858 m^2/gm and 590 m^2/gm were exhibited by activated carbon and silica gel respectively.. The AC revealed higher pore volume equal to 0.425 cm^3/gm compared to SG. The nearly same pore radii of 1.838 Å and 1.835 Å have been reported for AC and SG respectively.

Table 1. BET surface characterizations

Characteristics	Activated carbon	Silica gel
Single point surface area (m^2/gm)	858	590
Multipoint surface area (m^2/gm)	862	599
Micropore volume (cm^3/gm)	0.425	0.273
Pore radius (Å)	1.838	1.835

3.2. Activated Carbon (AC)

The reliance of sorption response (in terms of C/C_o) on time at different temperatures using AC (Wt.=180 gm) is depicted in Figure 2. The experiments were performed at a feed rate of 6.67 x 10^{-5} m^3/sec and carbon dioxide concentration of 0.05 (wt. fraction). The breakthrough time relies strongly on the temperature. The maximal breakthrough and saturation times of 870 sec and 1050 sec were realized at a temperature of 298 K. The breakthrough and saturation time declined to 725 sec and 915 sec on increasing the temperature at 308 K respectively. A reduced breakthrough time of 630 sec was attained at temperature of 318 K. Sorption temperature of 328 K attributed to reduced breakthrough and saturation times of 530 sec and 675 sec respectively. The prolonged breakthpoint time at decreased temperature signifies the enhanced capacity.

On the other hand, the breakthrough curve is vastly steep and it signifies the maximal utilization of the sorbent capacity. The utilization of maximal capacity at breakpoint is desired for economical separation for CO_2. The steepness of the response curve signifies the narrowness of metastable zone (MSZ). Narrow metastable zone attributes to faster adsorption. In all cases, minute differences in the width of meta-stable zone have been observed which indicate the almost same utilization of bed capacity at the breakthrough point. The lowest layer of the bed is nearly saturated and mostly the adsorption takes place over a comparatively narrow adsorption zone in which the concentration varies quickly. Narrow MTZ characterize the competent use of the adsorbent leads to reduced costs of energy regeneration.

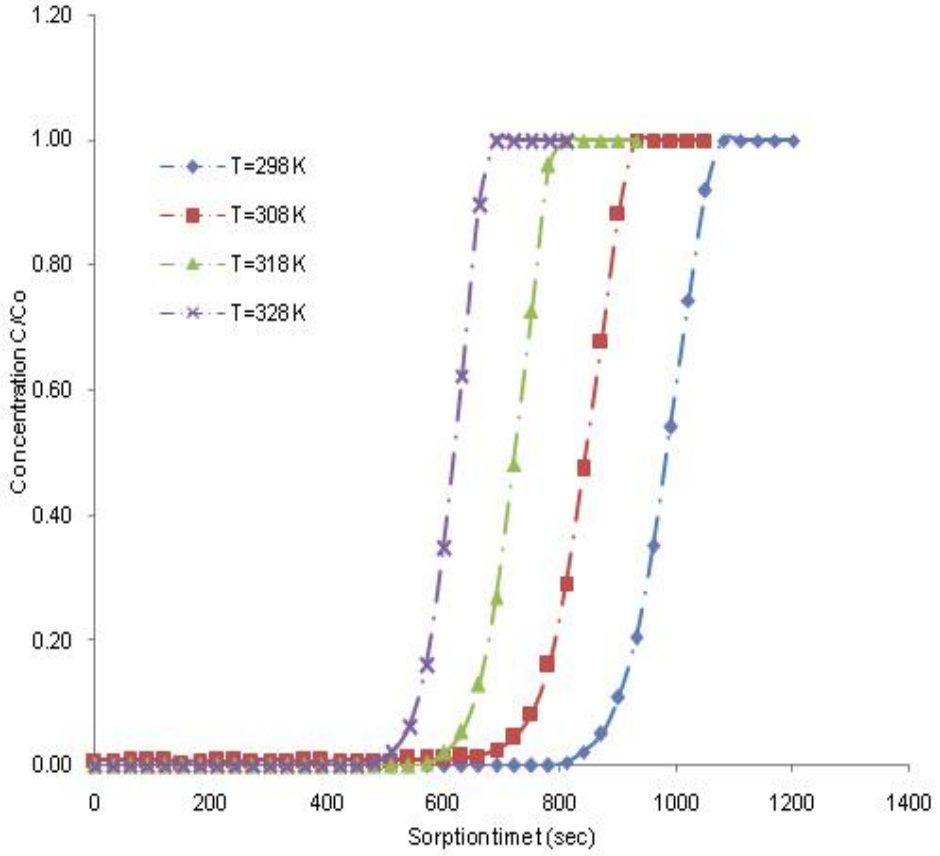

Figure 2. Breakthrough response for activated carbon for AC (F= 6.67 x 10^{-5} m^3/sec, CO_2 = 5%)

The sorption responses at various feed rates have been depicted in Figure 3. The feed rates of 5.00 x 10^{-5} m^3/s, 6.67 x 10^{-5} m^3/s and 8.33 x 10^{-5} m^3/s were selected at fixed temperature of 298 K. The breakthrough and saturation times vary significantly with feed rates. The prolonged breakpoint time of 1145 sec was attained at a feed rate of 5.00 x 10^{-5} m^3/sec. The breakpoint time reduced from 1145 sec to 975 sec on raising the feed rates from 5.00 x 10^{-5} m^3/sec to 6.67 x 10^{-5} m^3/sec. The minimal breakthrough and saturation times of 815 sec and 985 sec are exhibited by the AC at a feed rate of 8.33 x 10^{-5} m^3//sec. The saturation and breakthrough periods reduced considerably with increased feed flow rate.

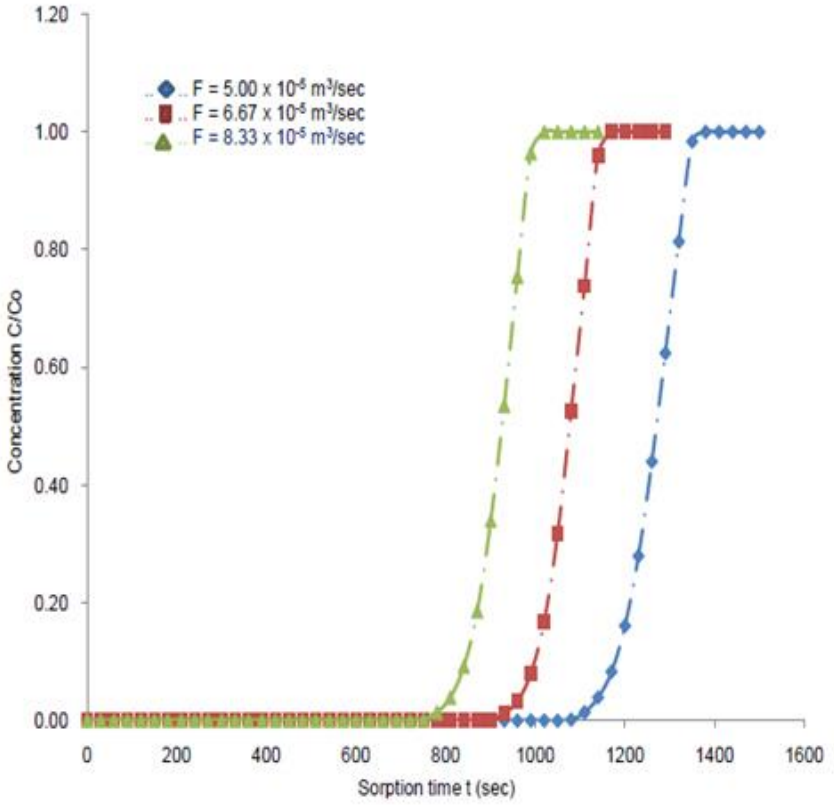

Figure 3. Breakthrough response at various feed rates for AC (T= 298 K, C_o = 5%)

Also, the narrow metastable zone exhibited by AC characterizes the suitability of carbon based adsorbent for carbon dioxide separation from CO_2/N_2 mixture. The steepness of the curve (S-shape) is very significant and highly desirable for economical adsorption. The mass transfer zone moves up the column as feed mixture flow. After the breakpoint time is approached, the concentration C raises very quickly upto the end of curve where the bed is judged unproductive.

The sorption capacity is estimated by dynamic mass balance which needs integration of the adsorption data. Utilizing the curve data, the time (t_s) equal to the total/ stoichiometric capacity is normally tabulated by integrating the following equation (Monazam *et al.*, 2013):

$$t_s = \int_0^{\infty} \left(1 - \frac{C}{C_o}\right) dt \qquad (1)$$

where, C is the CO_2 concentration at time t, C_o is the feed concentration of CO_2. Knowing t_s, the dynamic capacity q_t, of the bed can be calculated as (Serna-Guerrero and Sayari, 2010)

$$q_t = \frac{F\, t_s\, C_o}{m_{ad}} \qquad (2)$$

where, F is total feed molar flow rate, and m_{ad} is the mass of sorbent used in the bed. The portion of the column where adsorbate is really adsorbed on the sorbent is known as mass transfer zone (MTZ) length. The MTZ normally shifts from the inlet towards exit during the sorption operation. It means that the sorbent adjacent to inlet becomes saturated with the adsorbate and then the sorption zone towards the end-side of the bed. A schematic depiction of the response curve and shifting of the MTZ has been shown in Figure 4. The MTZ length was approximated assuming the constant pattern adsorption (Pota and Mathews, 1999):

$$L_{MTZ} = \frac{2L(t_s - t_b)}{t_s + t_b} \qquad (3)$$

Where L is the bed length; t_b and t_s stand for the breakthrough and saturation time (exhaustion time) respectively. These breakthrough and saturation times are the times corresponding to the outlet concentrations of 5 % and 95%. For assumed symmetric breakthrough curve, the bed capacity utilization can be estimated using utilization factor as:

$$f = 1 - \frac{0.5\, L_{MTZ}}{L} \qquad (4)$$

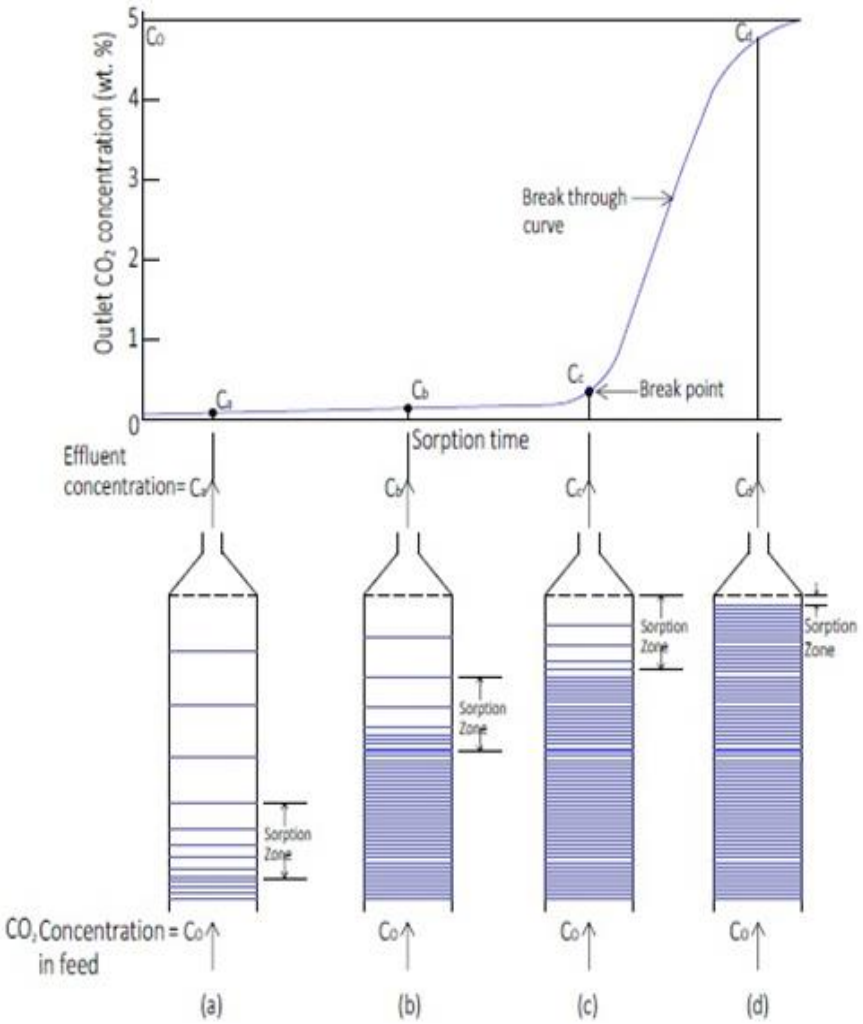

Figure 4. Breakthrough and mass transfer zone

The characteristics parameters i.e. saturation time, breakthrough time, length of the MTZ and capacity utilization factor were determined from the response curves (Figs. 2 and 3) for AC and depicted in Table 2. The breakthrough and saturation times decrease with increased temperature, leading to longer mass transfer zone. Also, breakthrough and saturation times reduce with feed flow rate resulting in increased length of MTZ. In common, the reduced temperature causes shorter MTZ owing to increased nucleation of product species. The length of MTZ increases with increased temperature and flow rate. The maximal length of MTZ equal to 5.78 cm was realized at T= 328 K and feed rate of F= 6.67 $x10^{-5}$ m^3/sec and reduced to 4.50 cm at a temperature of 298 K for AC. The utilization factor decreases with

increased sorption temperature and feed rate. The maximal value of f = 0.919 has been determined at T= 298 K and F= 5.00 x 10^{-5} m^3/sec.

Table 2. Effect of operating conditions on characteristics parameters for AC

T (K)	F, x10^{-5}(m^3/sec)	t_b (sec)	t_s (sec)	L_{MTZ} (cm)	f
298	6.67	870	1050	4.50	0.906
308	6.67	725	915	5.56	0.884
318	6.67	630	778	5.05	0.895
328	6.67	530	675	5.78	0.879
298	5.00	1145	1345	3.86	0.919
298	8.33	815	988	4.60	0.904

The CO_2 sorption capacity variation with temperature is predicted below (Figure 5). The data were obtained at a feed rate equal of 6.67 x 10^{-5} m^3/sec. The maximal capacity of 32.99 gm CO_2/Kg adsorbent was attained at a temperature of 298 K but reduced to 26.00 gm CO_2/Kg adsorbent at an increased temperature of 308 K. The capacity of 22.44 gm/Kg adsorbent was obtained at a temperature of 318 K. The temperature of 328 K contributed to a CO_2 capacity of 11.22 gm/Kg adsorbent. It was found that the maximal selective capacity of the adsorbent for CO_2 was strongly depended on the temperature and significantly reduced with increased temperature. The reduced temperature increases the capacity of CO_2 adsorption from CO_2 /N_2 feed mixture. The saturation adsorbent capacity varies significantly with bed temperature. The concentration of adsorbed gas or adsorption capacity lessened with increased temperature at a given equilibrium pressures, as adsorption is an exothermic process.

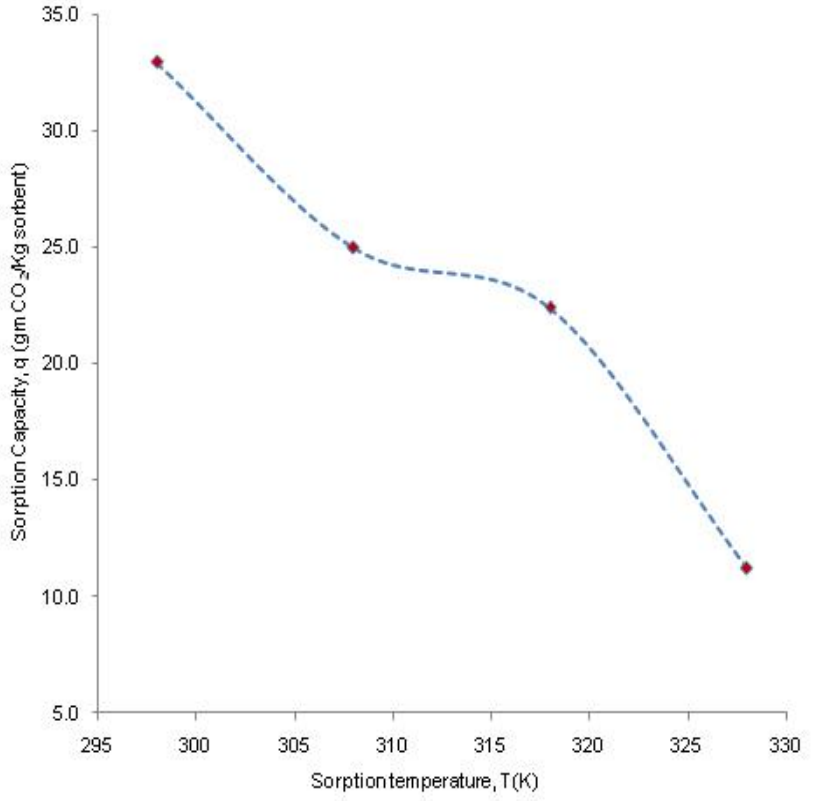

Figure 5. Sorption capacity vs. temperature curve for AC (F= 6.67 x10^{-5} m^3/sec, C_o=5%)

The adsorption isothers at a feed rate of 6.67 x 10^{-5} m^3/sec using activated carbon (AC) have been exhibited in Figure 6. The impact of different temperatures on sorption response was investigated at a fixed inlet CO_2 concentration of 5%. The capacity increases considerably with increased pressure of the CO_2. At a bed temperature of 298 K, the maximal adsorption capacity of 32.99 gm CO_2/Kg adsorbent was realized at an equilibrium partial pressure of 1.25 x 10^5 N/m^2. The capacity declined from 32.99 gm CO_2/Kg adsorbent to 12.20 gm/Kg adsorbent on reducing the CO_2 partial pressure from 1.25 x 10^5 N/m^2 to 0.50 x 10^5 N/m^2. At the same temperature (T=298 K), the adsorption capacity of 1.42 gm CO_2/Kg adsorbent was determined. For an adsorption isotherm produced at a bed temperature of 308 K, the minimal capacity of 1.09 gm CO_2/Kg adsorbent (P*= 0.062 x10^5 N/m^2) was exhibited by the adsorbent bed, and the capacity further enhanced to 20.14 gm/Kg adsorbent at a CO_2 pressure of 1.0 x 10^5 N/m^2. The sorption capacity of 22.441 gm/Kg adsorbent at a partial pressure of 1.25 x 10^5 N/m^2

was realized corresponding to a temperature of 318 K and capacity declined considerably to 10.34 gm CO_2/Kg adsorbent at a CO_2 pressure equal of 0.625 x10^5 N/m^2. The maximal and minimal capacities of 11.22 gm/gm adsorbent and 0.47 gm/Kg adsorbent have been exhibited at equilibrium partial pressures of 1.25 x 10^5 N/m^2 and 0.063 x 10^5 N/m^2 respectively at a temperature of 328 K.

Different gases are adsorbed to different extents under comparable conditions. It can be concluded that increasing the pressure of carbon dioxide will cause more of the adsorbable gas to be adsorbed as the rising curve indicates. It may be concluded that the adsorption capacity increases remarkably with partial pressure of the CO_2.

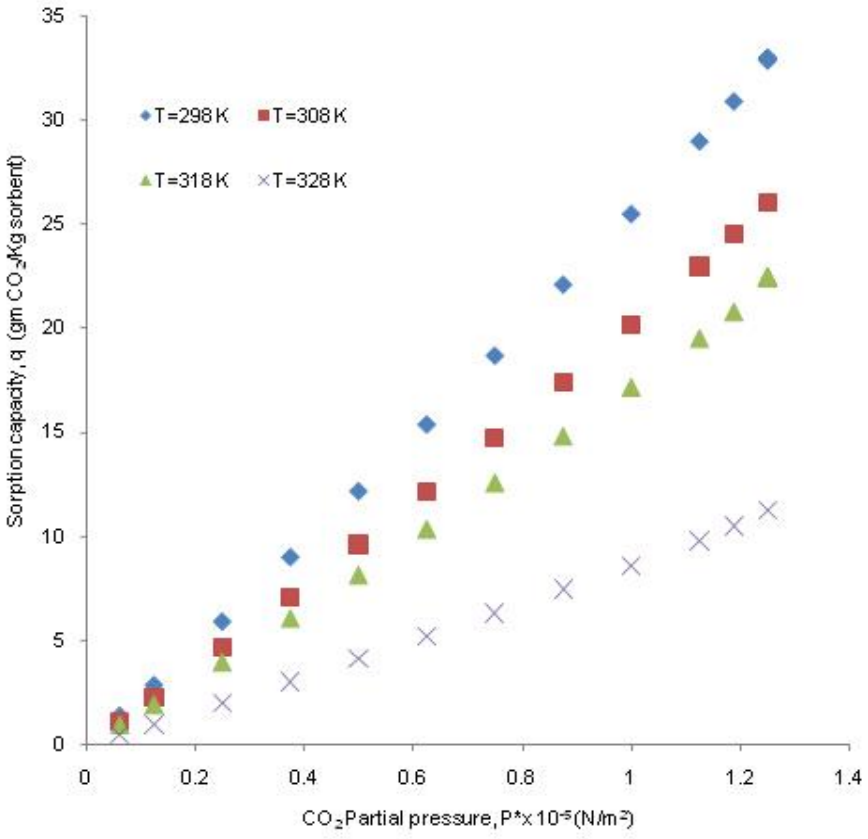

Figure 6. Sorption capacity vs. partial pressure curves for AC (F= 6.67 x10^{-5} m^3/sec)

The reliance of the feed rate on the capacity utilizing the AC from a CO_2/N_2 mixture has been depicted in Figure 7. The bed temperature was fixed at 298 K and the adsorbable gas concentration in feed

(CO_2) was adjusted at 0.05 (vol. %). The sorption capacity increases considerably with increased feed (N_2+CO_2) rate from 5.00 x 10^{-5} m^3/sec to 8.33 x10^{-5} m^3/sec. The capacity of 32.36 gm CO_2/Kg sorbent was realized at a feed rate of 5.00 x 10^{-3} m^3/sec and further enhanced to 36.39 gm CO_2/Kg sorbent on raising the feed rate at 6.67 x 10^{-5} m^3/sec. It was realized that as the increasing amount feed (fluid) are passed through the sorption column, the sorbent adsorbs an increasing amount of solute (CO_2) from the feed gas mixture yielding to increased sorption capacity. Therefore, it can be concluded that the capacity of the sorbent enhances significantly with increasing feed rates. The higher feed rate favors the increased sorption capacity of the adsorbed gas from the feed mixture (N_2+ CO_2).

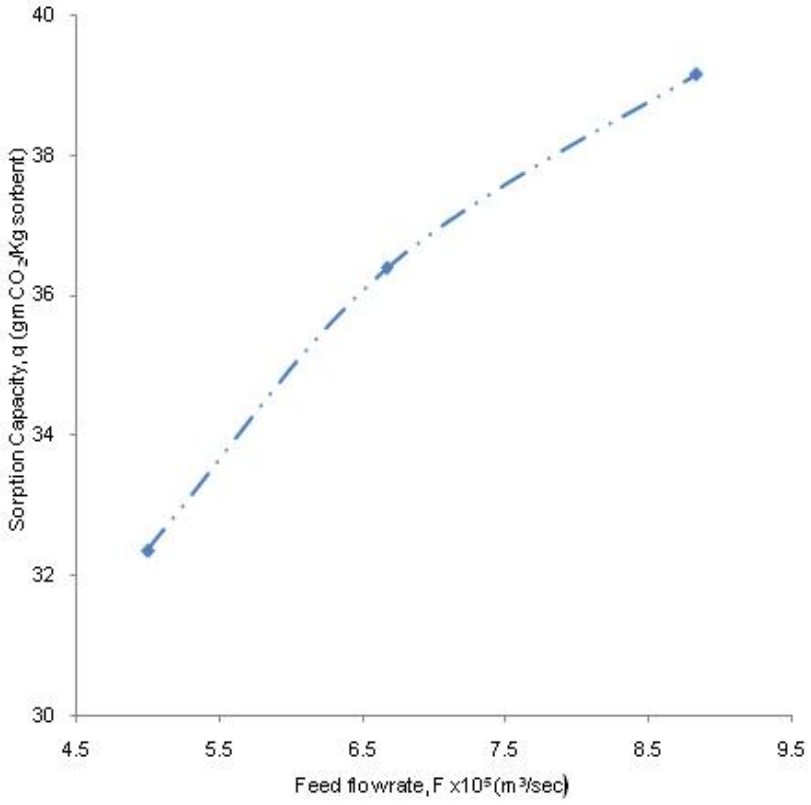

Figure 7. Sorption capacity vs. feed flow rate for AC (T=298 K)

The adsorption isotherms obtained at T= 298 K with feed rates ranging 5.00 x 10^{-5} m^3/sec to 8.33 x1 0^{-5} m^3/sec have been depicted in Figure 8. The capacity enhances with raised partial pressure of the adsorbable gas (CO_2). The capacity equal to 1.43 gm CO_2/Kg sorbent was obtained at a CO_2 pressure

of 0.063 x 10^5 N/m^2 and the capacity increased to 25.07 gm CO_2/Kg adsorbent on raising the CO_2 pressure at 1.0 x 10^5 N/m^2 at a feed rate of 5.00 x 10^{-5} m^3/sec. The maximal capacity equal to 32.36 gm CO_2/Kg sorbent was exhibited at a CO_2 partial pressure of 1.25 x 10^5 N/m^2. The increased capacity of 28.23 gm /Kg sorbent was determined at a CO_2 partial pressure equal to 1.0 x10^5 N/m^2 on fixing the feed rate at 6.67 x 10^{-5} m^3/sec. Generally, capacity improved remarkably with increased feed flow of the CO_2/N_2. The dependence of the capacity is more pronounced with adsorbable gas partial pressures compared to feed rates.

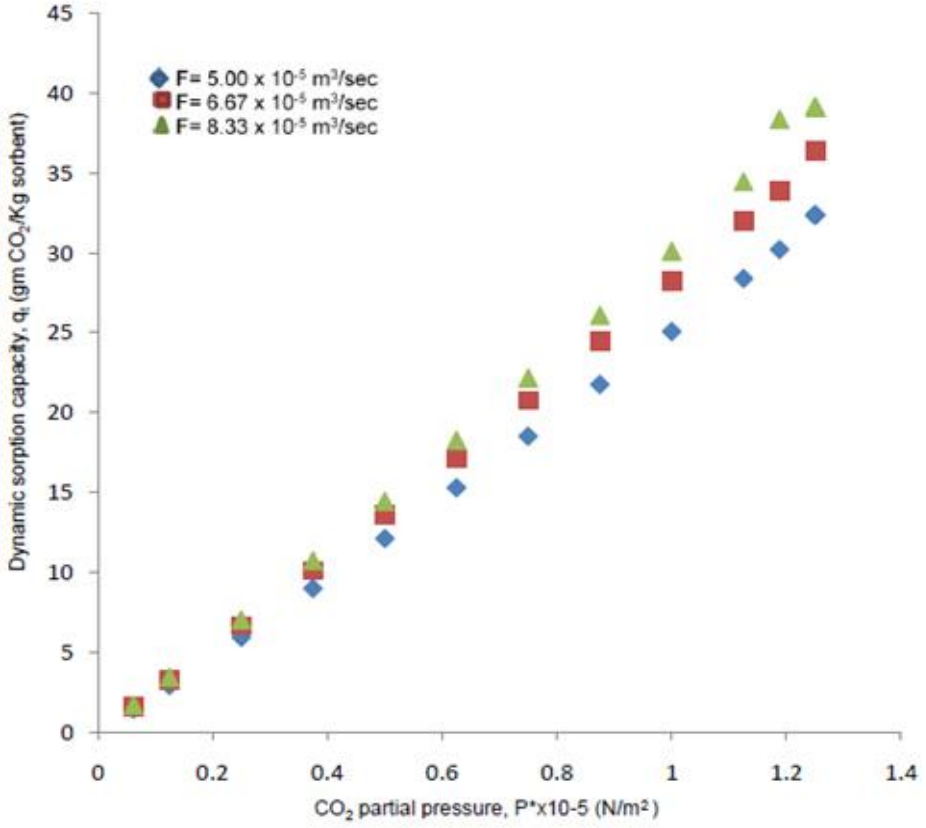

Figure 8. Sorption capacity vs. CO_2 partial pressure curve (T=298 K)

The temperature profiles of different temperature sensors (T1-T6) are depicted in Figure 9. Temperature sensors T7 (308 K) represent hot water circulator temperature. The temperature rise above the set point during initial sorption period attributes to the adsorption which is exothermic in nature and accompanied by liberation of heat. The temperatures T1 and T6 represent the top and bottom

temperatures respectively, whereas the temperatures T2–T5 correspond to the intermediate column temperature from the top to bottom side. All the temperatures sensors are insulated type-K thermocouples. Due to the exothermic nature of adsorption, the mass transfer front is followed by a rise in temperature that is supported by temperature profiles at different positions. Also, it was observed that as the concentration of CO_2, the heat generated due to adsorption leads to raised temperature inside the adsorption column.

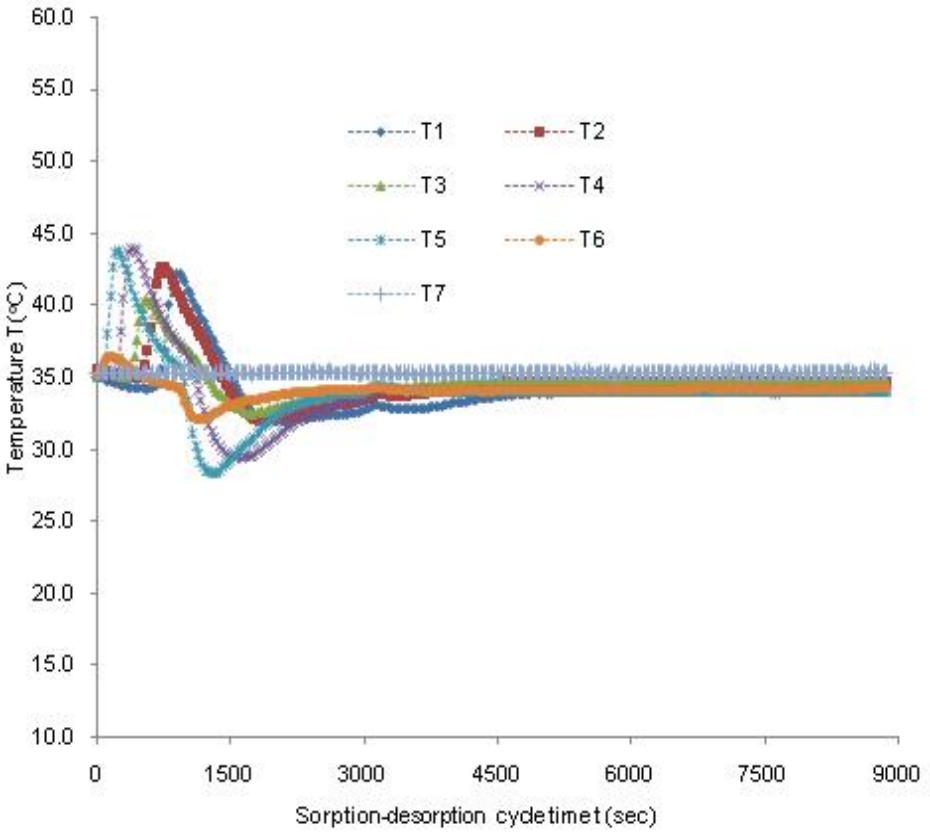

Figure 9. Temperature profiles inside the column of AC (F= 6.67 X 10^{-5} m^3/sec)

The accuracy was judged using the repeatability measurement. The repeatability is measured by generating the two sets of data at 298 K and feed rate of 5.00 x 10^{-5} m^3/sec. Closeness of the data depicted (Figure 10) indicates the reliability of the data. The R squared (R^2) has been found to be equal to 0.9962 and its value near to 1 signifies the good correlation among the repeated measurements. The data obtained for CO_2 adsorption is of high quality and reliable.

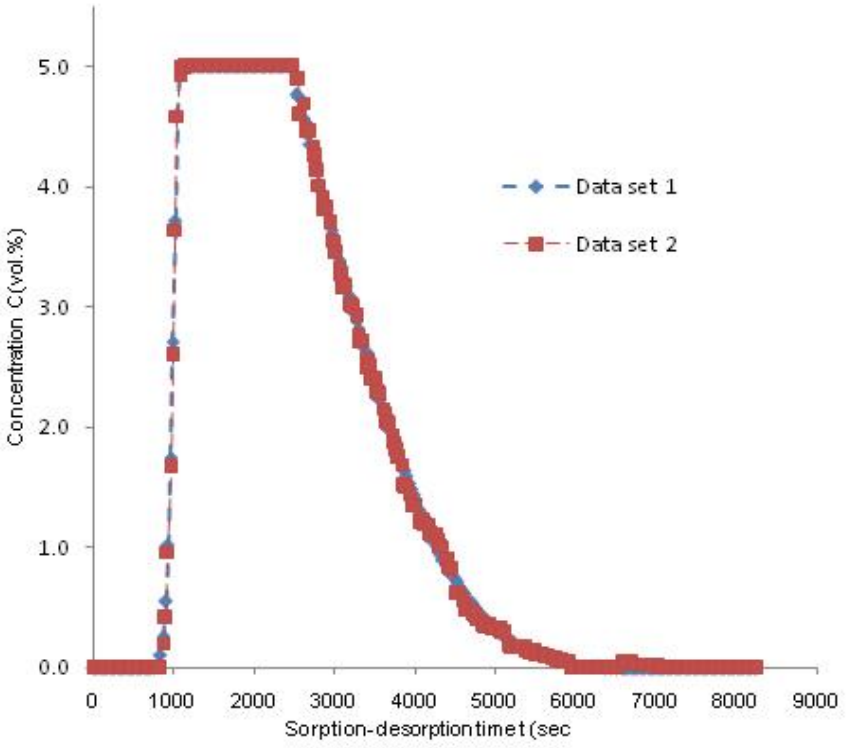

Figure 10 Repeatability measurement for AC (T= 298 K, F = 5.00 x 10^{-5} m^3/sec, CO_2 = 5%)

3.3. Silica gel (SG)

The response curves obtained at different temperatures using Silica gel (Wt.=275 gm) are depicted in Figure 11. The feed rate was controlled at 6.67 x 10^{-3} m^3/sec with initial CO_2 concentration fixed at 0.05 (vol/%). The sorption periods alter significantly with bed temperature. The breakthrough and saturation time of 195 sec and 350 sec were estimated as a temperature of 298 K. The breakpoint time reduced to 152 sec on raising the temperature to 308 K with saturation time of 290 sec. The temperature equal to 318 K contributed to a declined breakpoint and saturation times of 122 sec and 240 sec. The prolonged breakthrough and saturation time which characterize the improved capacity was reported for AC compared to SG. Under the same conditions of temperature i.e. 298 K and feed rate (6.67 x 10^{-5} m^3/sec), the breakpoint periods of 870 sec and 195 sec exhibited for AC and SG respectively. The breakpoint time reported for AC is almost more than 4 times of that reported for SG at fixed temperature (T=298 K) and feed rate (F= 6.67 x 10^{-3} m^3/sec).

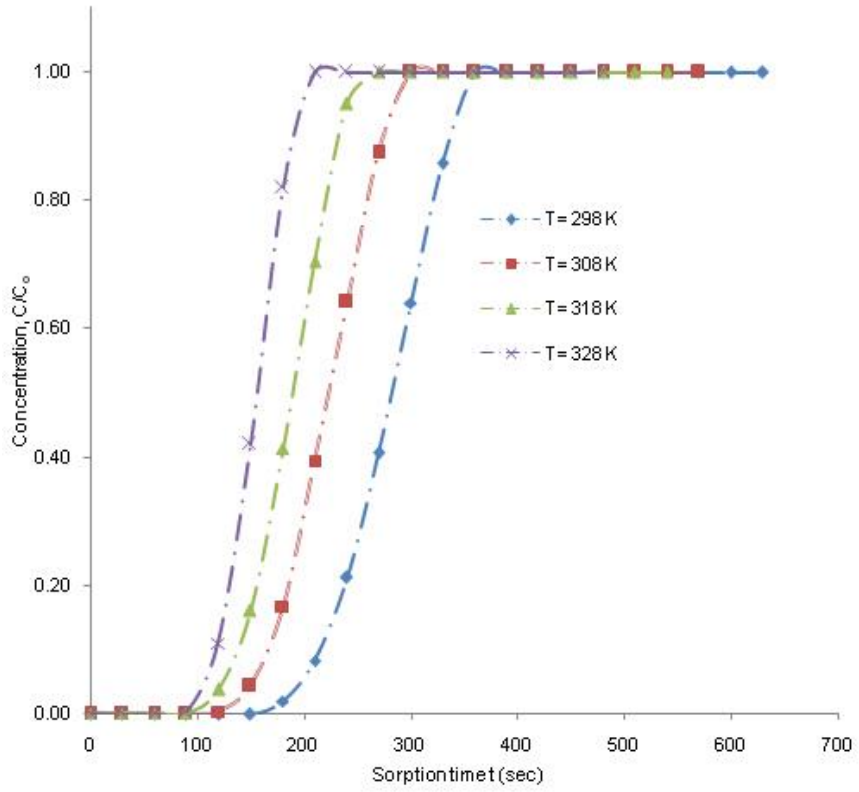

Figure 11. Sorption response at different temperatures for SG (F= 6.67 x 10^{-3} m^3/sec,CO_2= 5%)

The influence of feed rates on response of CO_2 separation utilizing SG has been predicted in Figure 12. The prolonged breakthpoint and saturation times of 250 sec and 425 sec are exhibited for SG adsorbent at a feed rate of 5.00 x 10^{-5} m^3/sec. The breakpoint time declined to 195 sec on increasing the feed rate to 6.67 x 10^{-5} m^3/sec. The saturation time of 370 sec was reported at a feed rate of 6.67 x10^{-5} m^3/s. The breakpoint and saturation time of 180 sec and 340 sec were achieved at a maximal feed rate of 8.33 x 10^{-5} m^3/sec.

The characteristics parameters of the CO_2 sorption determined from the breakthrough curves (Figures 11 and 12) for SG are depicted in Table 3. The breakthrough and saturation times reduce with increased temperature resulting in longer MSZ. Also, breakthrough and saturation time declines with increased feed flow rate resulting in increased length of MTZ. In general, the length of mass transfer zone (MTZ) increases with raised temperature and feed rate. The maximal vales of L_{MTZ} = 15.65 cm

was obtained at a temperature of 318 K and feed flow rate of 6.67 x10^{-5} m^3/sec. The utilization factor decreases with increased temperature and feel rate. The maximal utilization factor f= 0.740 has been determined at T= 298 K and F= 5.00 x 10^{-5} m^3/sec for SG.

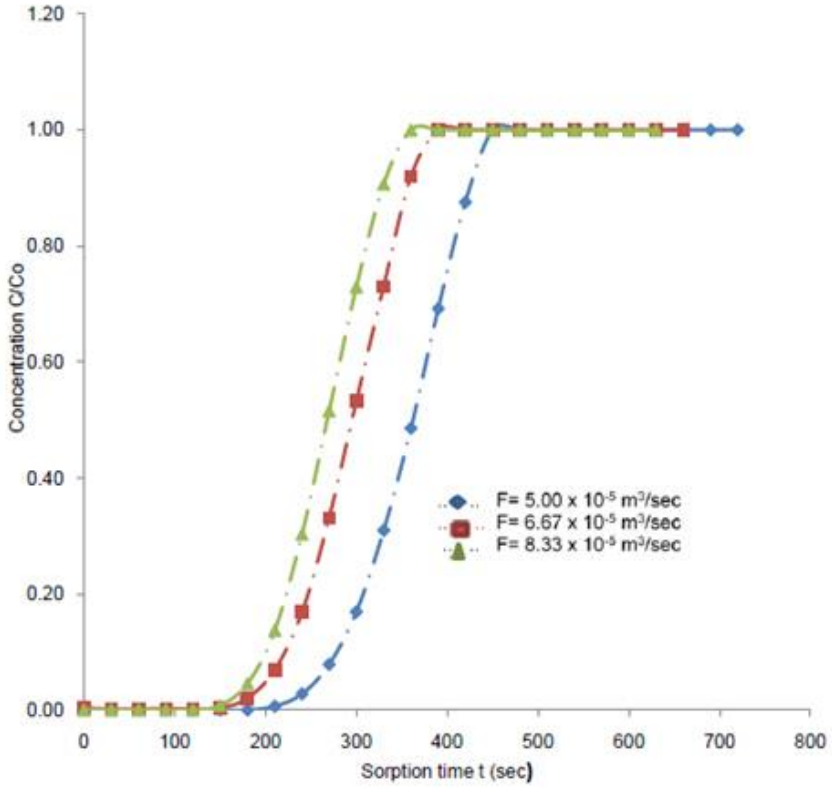

Figure 12 Sorption response at different feed rates for SG (T= 298 K, CO_2 = 5%)

Table 3. Effect of operating conditions on characteristics parameters for SG

T (K)	F, x10^{-5} (m^3/sec)	t_b (sec)	t_s (sec)	L_{MTZ} (cm)	f
298	6.67	195	350	13.65	0.706
308	6.67	152	290	14.99	0.688
318	6.67	122	240	15.65	0.674
328	6.67	105	206	15.59	0.675
298	5.00	250	425	12.44	0.740
298	8.33	180	340	14.77	0.692

The dependence of capacity on the temperature for SG is depicted in Figure 13. The data were generated at the superficial velocity of 6.67 x 10^{-5} m^3/sec. The capacity of reduced considerably with increased temperature. The maximal sorption capacity of 6.35 gm CO_2/Kg sorbent was attained at a temperature of 298 K and it declined to 4.95 gm CO_2/Kg sorbent on raising the temperature to 308 K. The temperature of 318 K contributed to a CO_2 capacity of 4.19 gm CO_2/Kg at similar operating conditions. The capacity further reduced to 3.30 gm CO_2/Kg adsorbent on raising the sorption temperature at 328 K. It was clearly demonstrated that the capacity of the adsorbable gas (CO_2) declined notably with increased temperature. The concentration of adsorbed gas or adsorption capacity lessened with increased temperature at a given equilibrium pressures. The capacity exhibited by the Silica gel (SG) is considerably lower compared to that obtained for activated carbon.

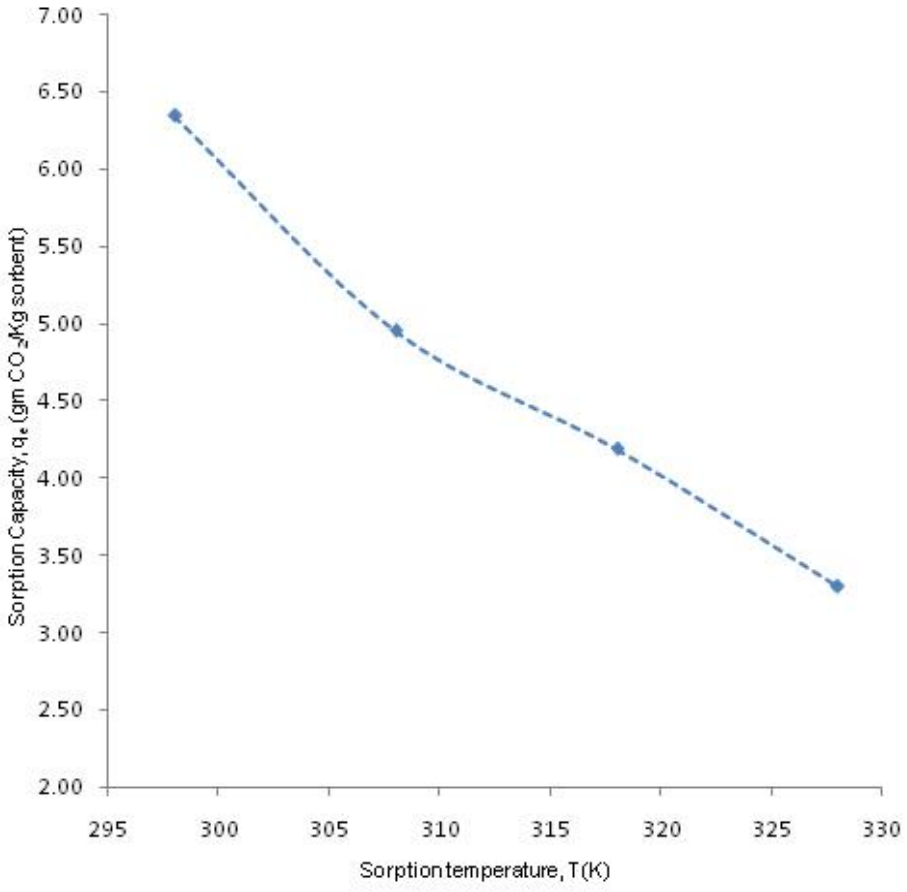

Figure 13 Sorption capacity vs. temperature curve for SG (Q= 6.67 x10^{-5} m^3/sec, C_o=5%)

The adsorption isotherms produced at different temperatures for SG have been depicted in Figure 14. The capacity increased considerably with increased CO_2 pressure. The capacity of 4.63 gm /Kg sorbent was determined at a carbon dioxide pressure of 1.0 $x10^5$ N/m^2 for isotherms generated at T= 298 K. At the same sorption temperature of T= 298 K, the minimal and maximal capacity of 0.20 gm CO_2/Kg sorbent and 6.35 g CO_2/Kg sorbent were attained at CO_2 partial pressures of 0.063 $x10^5$ N/m^2 and 1.250 x 10^5 N/m^2 respectively. The capacity of 4.95 gm CO_2/Kg sorbent was attained at fixed partial pressure of 1.25 x 10^5 N/m^2 with a temperature of 308 K. Similar trends of capacity variation with CO_2 partial pressure has been realized at an increased temperature of 318 K with a feed rate equal of 6.67 $x10^{-5}$ m^3/sec. The capacity further declined on raising the temperature to 328 K. The adsorption capacity of 1.0 gm CO_2/Kg sorbent was estimated at a CO_2 partial pressure of 0.5 x 10^5 N/m^2 and further increased to 2.76 g CO_2/Kg sorbent on raising the partial pressure at 1.13 $x10^5$ N/m^2.

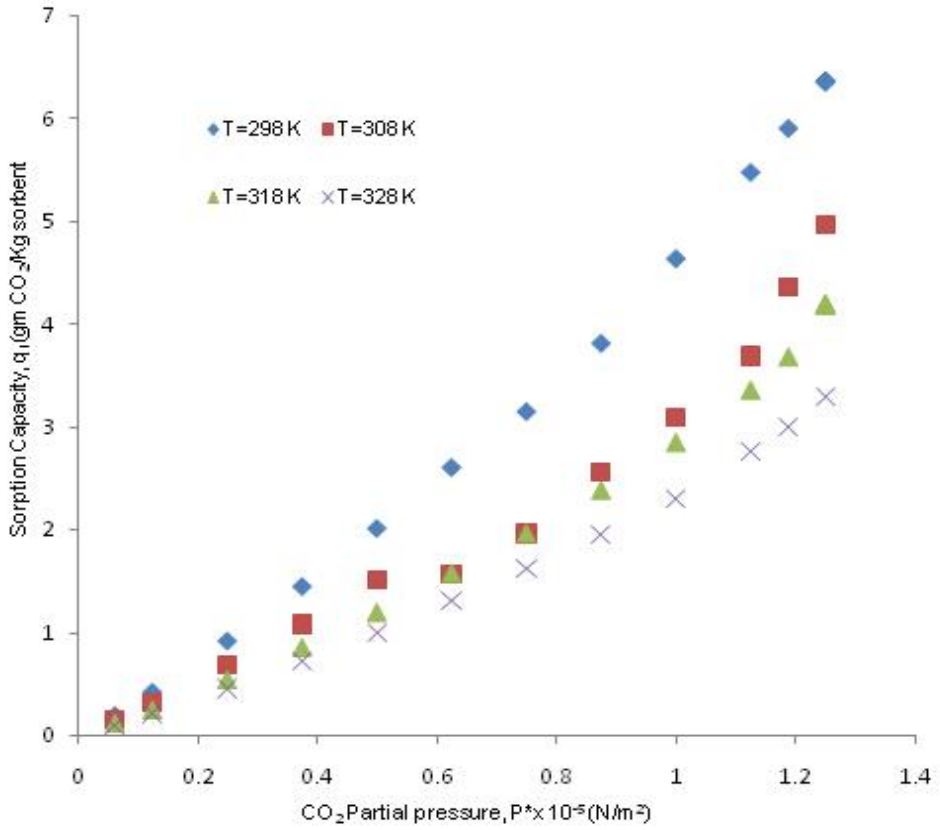

Figure 14. Sorption capacity vs. partial pressure curves for SG (F = $6.67x10^{-5}$ m^3/sec)

The impact of the feed rate on the capacity of CO_2 utilizing the SG from CO_2/N_2 mixture has been depicted in Figure 15. The temperature was fixed at 298 K and the CO_2 concentration was adjusted at 0.05 (vol. %). The capacity increases considerably with increased feed rate (N_2+CO_2). The capacity of adsorption of 5.91 gm CO_2/Kg sorbent was realized at the feed rate of 5.00 x10^{-5} m^3/sec. It was further increased to 6.78 gm CO_2/Kg sorbent on raising the feed rate to 6.67x 10^{-5} m^3/sec. The maximal capacity equal to 7.64 gm CO_2/Kg sorbent was attained at a feed rate of 8.33 x10^{-5} m^3/sec. It was realized that as the increasing amount of feed (fluid) are passed through the adsorption column, the adsorbent adsorbs an increasing amount of solute (CO_2) from the feed gas mixture resulting in increased adsorption capacity. Therefore, it can be concluded that the adsorption capacity of the sorbent enhanced significantly with feed rate. The higher feed flow favors the increased adsorption capacity of the adsorbed gas from the feed mixture (N_2+ CO_2). It is suggested that higher feed flow is advantageous for achieving the higher adsorption capacity.

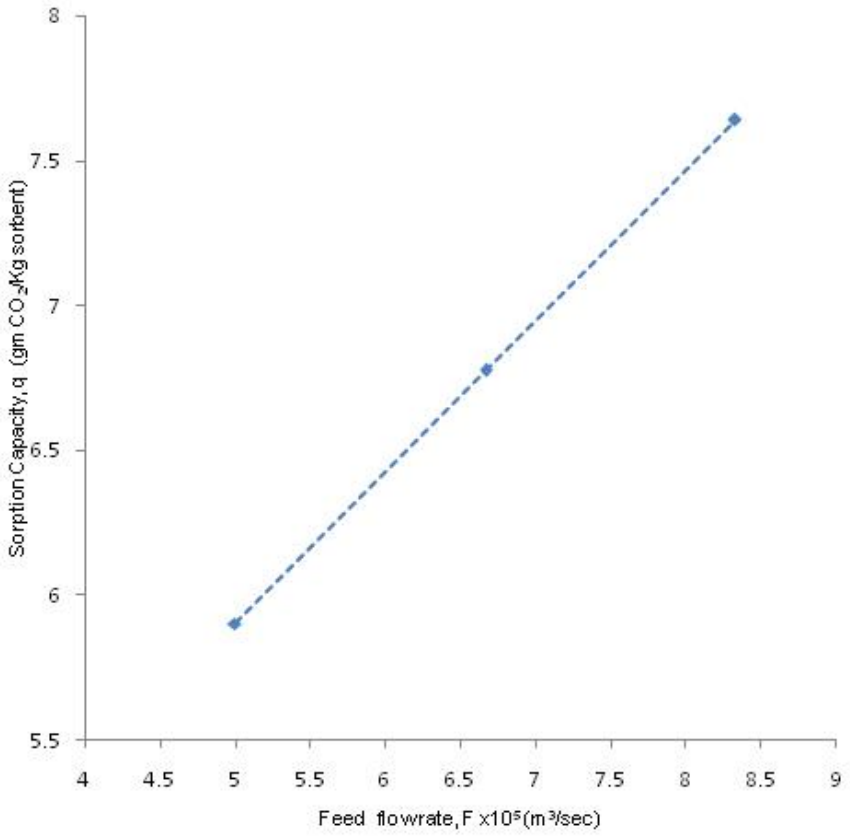

Figure 15 Sorption capacity vs. feed flow rate for SG (T = 298 K)

The adsorption isotherms obtained at T= 298 K at different feed rates have been depicted in Figure 16. The capacity improves with increased CO_2 pressure. The minimal capacity of 0.188 gm CO_2/Kg sorbent was realized at a CO_2 pressure of 0.06 x10^5 N/m^2 and the capacity increased to 1.49 gm CO_2/Kg sorbent on raising the pressure at 0.38 x10^5 N/m^2 under constant feed rate of 5.00 x1 0^{-5} m^3/sec. The maximal capacity equal to 5.91 gm CO_2/Kg sorbent was achieved at a CO_2 pressure of 1.25 x 10^5 N/m^2. The capacity increased of 4.85 gm /Kg sorbent was determined at a CO_2 partial pressure of 1.0 x10^5 N/m^2 and increased feed rate of 6.67 x10^{-5} m^3/sec. The maximal capacity improved to 6.78 gm CO_2/Kg sorbent at a partial pressure of 1.25 X10^5 N/m^2 under fixed rate of 6.67 x 10^{-5} m^3/sec. Generally, the sorption capacity of the sorbent improved remarkably with increased feed flow of the CO_2/N_2. The dependence of the sorption capacity is more pronounced with adsorbable gas partial pressures compared to feed rates.

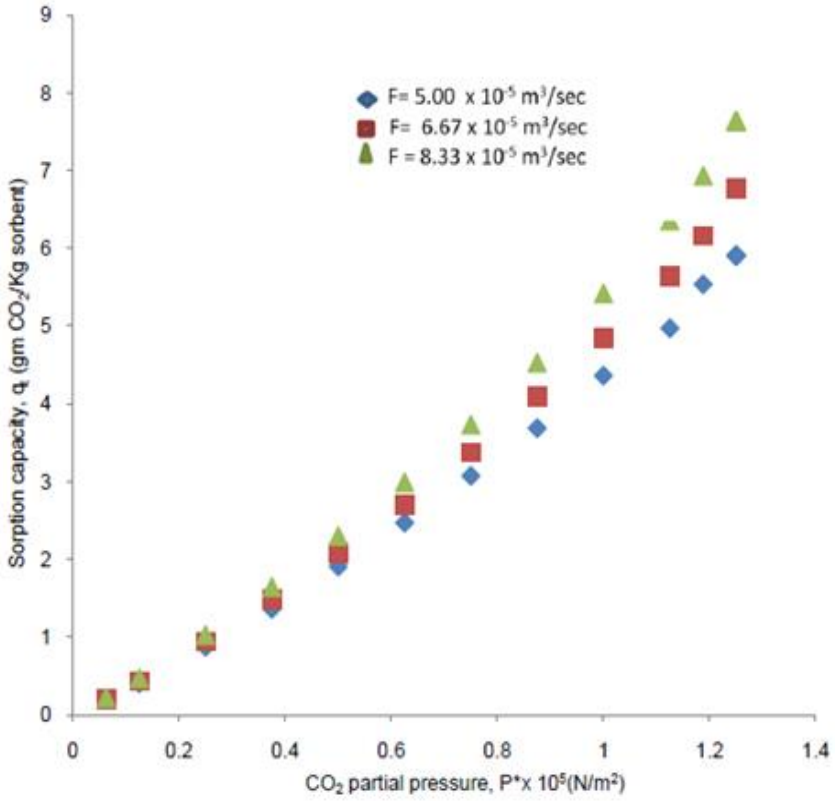

Figure 16. Sorption capacity vs. partial pressure for SG (T=298 K)

4. Conclusions

The sorption breakthrough time relies strongly on the sorption temperature and reduces with increased temperature. The maximal breakthrough and saturation periods of 870 sec and 1050 sec were exhibited for AC at a bed temperature of 298 K. The prolonged breakthrough and saturation times have been realized for AC compared to SG under constant operating conditions. The prolonged breakthrough time results in increased adsorption capacity. The breakthrough curves of AC are vastly steep signifying the maximal utilization of bed capacity at the breakpoint. Narrow MSZ characterize efficient use of the sorbent resulting in the reduction of costs of energy regeneration. The breakthrough and saturation times reduce significantly with increased feed rate and the prolonged breakpoint time of 1145 sec was attained at a feed rate of 5.00×10^{-5} m^3/sec for AC and these times are considerably higher than the values obtained for SG. In general, the length of MTZ increases with raised temperature and feed flow rate and maximal length of MTZ equal to 5.78 cm was determined at T= 328 K and F= 6.67×10^{-5} m^3/sec for AC. The utilization factor reduces with increased temperature and feed rate. The maximal utilization factors of 0.919 and 0.740 were determined at T= 298 K and F= 5.00×10^{-5} m^3/sec for AC and SG respectively signifying the relevance of AC for CO_2 separation. The CO_2 capacity strongly depends on the temperature and significantly reduces with an increased in bed temperature. The maximal capacities of 32.99 gm CO_2/Kg sorbent and 6.35 gm CO_2/Kg sorbent were determined at a temperature of 298 K for AC and SG respectively. The capacity improves considerably with raised pressure of the CO_2 and AC exhibited higher sorption capacity compared to SG at a lower adsorption temperature of 298 K and flow rate of 6.67×10^{-5} m^3/sec. The adsorption capacity increases considerably with increased feed rates ranging from 5.00×10^{-5} m^3/sec to 8.33×10^{-3} m^3/sec and maximal capacity of 39.14 g CO_2/Kg sorbent was determined for AC. The AC may be used for economical separation of CO_2 from N_2/CO_2 mixture owing to higher sorption capacity and utilization factor.

Acknowledgement

The research work was funded by the Deanship of Scientific Research (Project No. 310/1440), King Khalid University, Abha K.S.A.

References

Hester R.E., Harrision R.M., (2010), Carbon capture, Sequestration and storage. The Royal Society of Chemistry, Cambridge.

Li L., Zhao N., Wei W., Sun Y. (2013), A review of research progress on CO_2 capture, storage, and utilization in Chinese academy of sciences, *Fuel*, **108**,112-130.

Rashidi N.A., Yusuf S. (2016), An overview of activated carbons utilization for the post combustion carbon dioxide capture, *Journal of CO_2 Utilization*, **13**, 1-16.

IEA. (2003), CO_2 capture at power stations and other point sources. Zero emission technologies for fossil fuels. OECD/IEA, Cedex, France.

Lee S.Y., Park S.J. (2015), A review on solid adsorbents for carbon dioxide capture, *Journal of Industrial and Engineering Chemistry*, 23, 1-11.

IPCC (Intergovernmental panel on climate change). (2001), Climate change, Synthesis report, Cambridge University Press, Cambridge, UK.

Alabadi A., Razzaque S., Yang Y., Chen S., Tan B. (2015), Highly porous activated carbon materials from carbonized biomass with high capturing capacity, *Chemical Engineering Journal*, **281**, 606-612.

Figueroa J.D., Fout T., Plasynski S., Mcllcried H., Srivastava R.D. (2008), Advances in CO_2 capture technology-The US department of energy's carbon sequestration program, *International Journal of Greenhouse Gas Control*, **2**, 9-20.

Gibbins J., Chalmers H. (2008) , Carbon capture and storage, *Energ Policy* ,**36**, 4317-4322.

Blomen E., Hendriksa C., Neele F. (2009), Capture technologies: improvement and promising developments, *Energy Procedia*, **1**, 1505-1512.

Choi W.J., Seo J.B., Jang S.Y., Jung J.G., Oh K.J.(2009), Removal characteristic of CO_2 using aqueous MEA/AMP solutions in absorption and regeneration process, *Journal of Environmental Science*, **21**, 907-913.

Gomes J., Santos S., Bordado J. (2015), Choosing amine based adsorbents for CO_2 capture, *Environmental Technology*, **36**, 19-25.

Gupta M., Coyle I., Thambimuthu K. (2003), Strawman document for CO_2 capture and storage technology roadmap. Canmet Energy Technology Centre, Natural Resources, Canada.

Brunetti A., Scura F., Barbieri G., Drioli E. (2010), Membrane technologies for CO_2 separation, *Journal of Membrane Science*, **359**,115-125.

Yang H., Xu Z., Fan M., Gupta R., Slimane R.B., Bland A.E., Wright I. (2008), Progress in carbon dioxide separation and capture: a review, *Journal of Environmental Science*, **20**, 14-27.

MacDowell N., Florin N., Buchard A., Hallett J., Galindo A., Jackson G., Adjman C., Williams C.K., Shah N., Fennel P. (2010), An overview of carbon dioxide capture technologies, *Energy and Environmental Science*, **3**, 1645-1669.

Cohen S.M., Chalmers H.L., Webbe M.E., King C.W. (2011), Comparing post-combustion carbon dioxide capture operation at retrofitted coal-fired power plants n the Texas and Great Britain electric grids, *Environmental Research Letters*, **6**, 1-14.

Garcia S., Gil M.V., Martin C.F., Pis J.J., Rubiera F., Pevida C. (2011), Breakthrough adsorption study of a commercial activated carbon for pre-combustion carbon dioxide capture, *Chemical Engineering Journal*, **171**,549-556.

Valverde J.M., Pontiga F., Soria-Hoyo C., Quintanlla M.A.S., Moreno H., Duran F.J., Espin M.J. (2011). Improving the gas solids contact efficiency in a fluidized bed of carbon dioxide adsorbent fine particles, *Physical Chemistry Chemical Physics*, **13**, 14906-14909.

Li J., Ma Y., McCarthy M., Sculley J., Yu J., Jeong H., Balbuen P., Zhou H. (2011), Carbon dioxide-related gas adsorption and separation in metal-organic frameworks, *Coordination Chemistry Reviews*, **255**, 1791-1823.

Alonso M., Rodriguez N., Gonzalez B., Grasa G., Murillo R., Abanades J.C. (2010). Carbon dioxide capture from combustion flue gases with a calcium oxide chemical loop: Experimental results and process developments, *International Journal of Greenhouse Control*, **4**,167-173.

Raganati F., Ammendola P., Chirone R. (2015), CO_2 capture by adsorption on fine activated carbons in a sound assisted fluidized bed, *Chemical Engineering Transactions*, **43**,1033-1038.

Abanadas J.C., Anthony E.J., Lu D.Y., Salvador C., Alvarez D. (2004), Capture of carbon dioxide from combustion gases in a fluidized bed of calcium oxide, *AIChE Journal*, **50**, 1614-1622.

Valverde M., Duran F.J., Pontiga F., Moreno H. (2012), CO_2 capture by enhancement in a fluidized bed of a modified Geldart C powder, *Powder Technology*, **224**, 247-252.

Shen C., Yu J., Li P., Grande C.A., Rodrigues AE (2011) Capture of CO_2 from flue gas by vacuum pressure swing adsorption using activated carbon beads, *Adsorption*, **17**, 179-188.

Sarkar A.I., Aroonwilas A., Veawab A. (2017), Equilibrium and kinetic behavior of CO_2 adsorption onto zeolites, carbon molecular sieve and activated carbons, *Energy Procedia*, **114,** 2450-2459.

Al-Janabi N., Vakili R., Kalumpasut P., Gorgojo P., Siperstein F.R., Fan X. (2018), Velocity variation effect in fixed bed columns: a case study of CO_2 captures using porous solid adsorbents, *AIChE Journal*, **64**, 2189-2197.

Shen C., Grande C.A., Li P., Yu J., Rodrigues A.E. (2010), Adsorption equilibria and kinetics of CO_2 and N_2 on activated carbon beads, *Industrial and Engineering Chemistry Research*, **47**, 4883-4890.

Xiang S., He Y., Zhang Z., Wu H., Zhou W., Krishna R., Chen B. (2012), Microporous metal-organic framework with potential for carbon dioxide capture at ambient conditions, *Nature Communications*, **3**,1-9.

Yoro K.O., Singo M., Mulopo J.L., Daramola M.O. (2017), Modeling and experimental study of the CO_2 adsorption behavior of polyaspartamide as an adsorbent during post-combustion CO_2 capture, *Energy Procedia*, **112**, 1643-1664.

Lu C., Bai B., Wu B., Su F., Hwang J.F. (2008), Comparative study of CO_2 capture by carbon nanotubes, activated carbons, and zeolites, *Energy Fuels*, **22**, 3050-3056.

Al Mesfer M.K., Danish M., Fahmy M.Y., Rashid M.M. (2018), Post combustion CO_2 capture with activated carbons using fixed bed adsorption, *Heat Mass Transfer*, **54**, 2715-2724.

Al Mesfer M.K., Danish M. (2018), Breakthrough adsorption study of activated carbons for CO_2 separation from flue gas, *Journal Environmental Chemical Engineering*, **6**, 4514-4524.

Dejang N., Somprasit O., Chindaruksa S. (2015), A preparation of activated carbon from Macadamia shell by microwave irradiation activation, *Energy Procedia*, **79**, 727-732.

Jahangiri M., Shahtaheri S.J., Adl J., Rashidi A., Kakooei H., Forushani A.R., Nasiri G., Ghorbanali A., Ganjali M.R. (2012), Preparation of activated carbon from walnut shell and its utilization for manufacturing organic-vapor respirator cartridge, *Fresenius Environmental Bulletin*, **21**,1508-1514.

Calvo-Munoz E.M., Garcia-Mateos F.J., Rosas, Rodrigues-Mirasol J., Cordero T. (2016), Biomass waste carbon materials as adsorbents for CO_2 capture under post-combustion conditions, *Frontiers in Materials*, *3*,1-14.

Toprak A., Kopac T. (2017), Carbon dioxide adsorption using high surface area activated carbons from local coals modified by KOH, NaOH and $ZnCl_2$ agents, *International Journal of Chemical Reactor Engineering*, **15**,1-16.

Dantas T.L.P., Amorim S.M., Luna F.M.T., Silva Jr. I.J., Azevedo D.C.S., Rodrigues A.E., Morera R.F.P.M. (2010), Adsorption of carbon dioxide onto activated carbon and nitrogen-enriched activated carbon-surface changes, equilibrium, and modeling of fixed bed adsorption, *Separation Science and Technology*, **45**,73-84.

Regufe M.J., Ferreira A.F.P., Lourero J.M., Shi Y., Rodrigues A., Ribeiro A.M. (2018), New hybrid composite honeycomb monolith with 13X zeolite and activated carbon for CO_2 capture. *Adsorption*, **24**, 249-265.

Qasem N.A., Ben-Mansour R., Habib H.A. (2017), Enhancement of adsorption carbon capacity of 13X with optimal incorporation of carbon nanotubes, International Journal of Energy and Environment, 8, 219-230.

Plaza M.G., Duran I., Querejeta N., Rubiera F., Pevida C. (2016), Experimental and simulation study of adsorption in post combustion conditions using a microporous biochar.1. CO_2 and N_2 adsorption, *Industrial and Engineering Chemistry Research*, **55**, 3097-3112.

Zhang Z., Wang B., Sun Q. (2014), Fly Ash– derived solid amine sorbents for CO_2 capture from flue gas, *Energy Procedia*, **63**, 2367-2373.

Hidayu A.R., Muda N. (2017), Impregnated Palm kernel shell activated carbon for CO_2 adsorption by pressure swing adsorption, *Indian Journal of Science Technology*, **10**, 1-6.

Patil P., Singh S., Kumar Y.M. (2013). Preparation and study of properties of activated carbons produced from agricultural and industrial waste shells, *Research Journal of Chemical Sciences*, **3**, 12-15.

Xia H., Cheng S., Zhang L., Peng J. (2016), Utilization of walnut shell as a feedstock for preparing high surface area activated carbon by microwave induced activation: effect of activation agents, *Green processing and synthesis*, **5**, 1-21.

Mataji M., Khoshandam B. (2014), Benzene adsorption on activated carbon from walnut shell, *Chemical Engineering Communications*, **201**, 1294-1313.

Monazam E.R., Spenik J., Shadle L.J. (2013), Fluid bed adsorption of carbon dioxide on immobilized polyethylenimine (PEI): kinetic analysis and breakthrough behaviour, *Chemical Engineering Journal*, **223**, 795-805.

Serna-Guerrero R., Sayari A. (2010), Modeling adsorption of CO_2 on amine functionalized mesoporous silica. 2: kinetics and breakthrough curve, *Chemical Engineering Journal*, **161**, 182-190.

Pota A.A., Mathews A.P. (1999), Effect of particle stratification on fixed bed adsorber performance, Journal of Environmental Engineering, **8**, 705-711.